



Dynamic modeling of flux and total hydraulic resistance in nanofiltration treatment of regeneration waste brine using artificial neural networks

Fakhreddin Salehi, Seyed M.A. Razavi*

Department of Food Science and Technology, Ferdowsi University of Mashhad, Khorasan, P.O. Box 91775-1163, Mashhad, Iran

Tel. +98 511 8795620; Fax: +98 511 8787430; email: s.razavi@um.ac.ir

Received 7 May 2011; Accepted 25 January 2012

ABSTRACT

Artificial neural networks (ANNs) were used to predict dynamically the permeate flux and total hydraulic resistance through the crossflow nanofiltration (NF) of waste brine. The ANN was fed with three inputs: transmembrane pressure (TMP), temperature and time. It was found that ANN with 1 hidden layer comprising nine neurons gives the best fitting with the experimental data, which made it possible to predict flux and total hydraulic resistance with high correlation coefficients (0.96 and 0.98, respectively). The effect of TMP and temperature on the recovery of useable brine from waste brine was also investigated by using polyamide tubular NF membrane. High reduction in salt and water consumption was achieved in this study. In addition, experimental results showed that the flux was increased significantly with increase in pressure and temperature ($p < 0.01$), whereas fouling and NaCl rejection increased considerably as the pressure and temperature increased, respectively. With an increase in TMP and temperature, it was observed that total hydraulic resistance, gel layer resistance and concentration polarization resistance were increased. Pressure was the most sensitive factor for prediction of both flux and total hydraulic resistance.

Keywords: Membrane; Simulation; Wastewater treatment; Hydraulic resistances

1. Introduction

At some sugar refineries, removal of color from sugar liquor using anion exchange resin is practiced. The colorants are first adsorbed onto the resins and then released from the regenerated resin into alkaline 100 g/l sodium chloride solution, producing a stream characterized by high salinity, high amount of colored organic matter and high COD (13,000 mg/l) [1–2]. This waste brine stream usually poses a disposal problem. The organic matter in the regeneration effluent con-

sists of natural sugarcane pigments (mostly phenolic compounds) and colorants that are formed during the cane juice processing. The molar mass of the compounds ranges from less than 500 g/mol to more than 20,000 g/mol, with most of the color being due to the compounds in the 5,000–20,000 g/mol range. The compounds are mostly negatively charged, with up to six or more functional groups conveying the negative charges on each species [3].

Membrane separation process in water treatment has gradually gained popularity because it effectively removes a variety of contaminants from raw waters. While microfiltration (MF) and ultrafiltration (UF)

*Corresponding author.

membranes can mainly remove suspended particles and macromolecules, nanofiltration (NF) membranes are an effective technology to remove dissolved organic contaminants with molecular weights (M_w) larger than 200 Da and about 70% of monovalent ions by electrostatic repulsion (charge effect), size exclusion (sieving effect) and a combination of the rejection mechanisms. Diffusion, sieving, convection and other mechanisms can affect mass transport in membrane processes [4–6].

According to previous findings, the NaCl retention of NF membranes is as low as 10–50%, while organic compounds retention has been reported by Wadley et al. [3] in 1995 to be in the range of 80–97% on Koch NF membranes (SelRO MPT-30 or MPT-31). It has also resulted in 30% reduction of effluent volume and 60% reduction in salt consumption. In 1997, Cartier et al. [2] referred that with spiral wound membranes Desal 5.1 and Desal 5.2 (today Osmonics) and Filmtec NF4S membrane (Dow), it is possible to reach even 89 and 74% reduction in water and salt consumptions, respectively. Based on the resistance-in-series model, some researchers proposed experimental methods to analyze membrane fouling phenomenon [7].

Dynamic modeling of membrane process is very important for designing of a new process and better understanding of the present process. ANN can be used for mapping input and output data without knowing information between them [8]. In the field of membrane separation processes, ANNs have successfully been applied to different types of membranes including MF, UF and NF [5]. Literature review shows that ANNs were used to predict the performance of membrane systems in terms of permeate flux, membrane fouling, time evolution of membrane fouling, total hydraulic resistance and components rejection and ANNs offer a more attractive alternative to conventional black box models in dealing with complex phenomena [9–14]. However, there is no study available in the literature concerning the use of ANN for dynamic modeling of permeate flux and total hydraulic resistance of NF of high salt concentration (100 g/l).

The objectives of present paper were (i) to study the effect of operating parameters on dynamic permeate flux and total hydraulic resistance of polyamide membrane during NF of waste brine from resin regeneration, (ii) to develop and validate the application of neural networks for the dynamic modeling of permeate flux and total hydraulic resistance as a function of transmembrane pressure (TMP) and temperature, and (iii) to evaluate the performance of NF for recovery of brine and water of waste brine in order to reuse and reduction in effluent volume.

2. Materials and methods

2.1. Membrane setup

Fig. 1 shows a schematic diagram of the NF pilot-plant system used in this study. The polymeric tubular AFC40 membrane was supplied by PCI membrane systems, UK. The characteristics of NF membrane are summarized in Table 1. Permeate solutions were collected in a beaker, and were not returned into the feed tank, whereas the retentate was circulated back to the feed tank. A permeate collection vessel, located on an electronic balance (± 0.05 g), was used to collect permeate and measure permeate flux ($\text{kg}/\text{m}^2\text{s}$) during the experiments. All the experiments were carried out at 60 min. Since the feed volume was continuously reduced in the concentration mode of filtration tests, the fluxes also declined continuously. Volume reduction factor (VRF) was calculated using the following equation:

$$\text{VRF} = \frac{V_f}{V_c} \quad (1)$$

where V_f and V_c are the initial volume of feed and the final volume of the concentrate, respectively.

2.2. Experimental procedure

The operating pressure of each run was at the range of 1.0–2.0 MPa (at three levels of 1.0, 1.5 and 2.0 MPa). While the temperature was varied from 30–50°C (at three levels of 30, 40 and 50°C) and controlled by a tubular heat exchanger. Ion-exchange res-

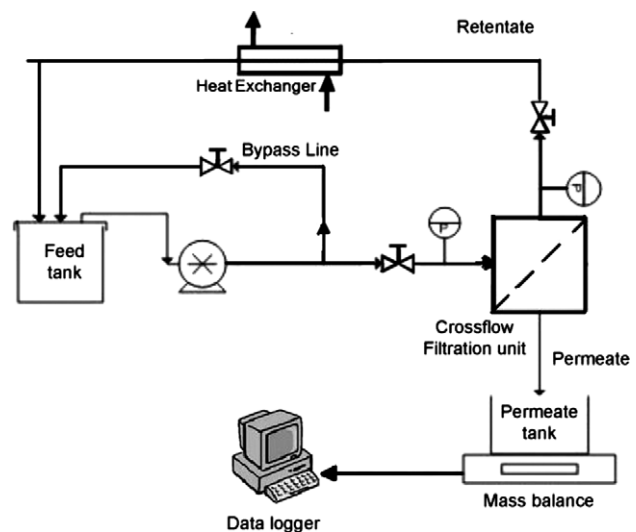


Fig. 1. Schematic diagram of the tubular NF pilot plant system used in this study.

Table 1
Characteristics of NF membrane and module used in this study

Membrane type	AFC40 (PCI Membranes Ltd., UK)
Material	Polyamide film
Effective area	240 cm ²
Diameter	63.5 mm
Length	30 cm
Range of pH tolerance	1.5–9.5
Maximum temperature	60°C
Maximum pressure	6 MPa
Apparent retention character	60% CaCl ₂
Module	Tubular (Micro 240) (PCI Membranes Ltd., UK)

ins effluent (concentration 100 g/l) from sugar decolorizing column obtained from a sugar plant (Sepid-Mehr sugar beet factory, Neyshabur, Iran) and this batch used as the NF feed in all runs. The wastewater and all samples were refrigerated at 4°C. The pH of feed solutions was constant and obtained averagely 7.8 ± 0.1 .

Optical density (OD) was chosen as a measure for the colorant concentration in permeates and retentate samples [2]. OD was measured at 420 nm and 25°C using a UV-vis spectrophotometer (Jenway 6105, Bibby Scientific Limited, UK). In order to determine the concentration of sodium chloride in the retentate and the permeate samples the conductivity of the samples was measured by a conductivity meter (Jenway 4010, Bibby Scientific Limited, UK). Dynamic viscosity of permeate samples was determined using an Ostwald U-tube capillary viscometer at 20°C after each NF run. All NF operations and experiments were carried out in two replications and the results were averaged.

2.3. Membrane performance parameters

The rejection of sodium chloride and dye compounds was calculated by the following equation:

$$R = \left(1 - \frac{C_p}{C_f}\right) \times 100\% \quad (2)$$

where, R is the rejection, C_p and C_f are the concentration of each component (g/l) in the permeate and feed streams, respectively. During the transport of solutes from the feed solution to the membrane surface, solute concentrations at the membrane surface are higher than in the feed solution, leading to concentration

polarization. In some cases, solute concentrations at the membrane surface can reach a limiting value. In these conditions, a gel layer begins to accumulate, leading to surface and/or internal pore fouling [15]. The fouling mechanisms, including concentration polarization, gel layer formation and pore blocking, introduce additional resistances to transport across the membrane due to the increased osmotic pressure on the feed side [16]. Membrane fouling was determined as:

$$\text{Fouling} = \left(\frac{J_w - J_{wf}}{J_w}\right) \times 100\% \quad (3)$$

where, J_w and J_{wf} is the flux of distilled water through a membrane before and after each run, respectively. To understand the flux decline in pressure-driven membrane operations, a number of models were developed. Two of the most widely studied models are the resistance-in-series model and the concentration polarization model. In this study, the hydraulic resistances were calculated by applying the resistance-in-series model, containing intrinsic membrane resistance (R_m), gel layer resistance (R_g) and concentration polarization resistance (R_{cp}), as follows [17].

$$R_T = R_m + R_g + R_{cp} \quad (4)$$

The total hydraulic resistance (R_T) is defined as:

$$R_T = \frac{\text{TMP} - \Delta\pi}{\mu_p J_p} \quad (5)$$

where μ_p and J_p are the permeate viscosity and flux, respectively. In this study, the passage of sodium chloride ion through the membrane was high (low rejection of NaCl), it was assumed that the osmotic pressure difference ($\Delta\pi$) is small. Transmembrane pressure (TMP) can be calculated by the following equation:

$$\text{TMP} = \frac{P_i + P_o}{2} - P_p \quad (6)$$

where, P_i and P_o are inlet and outlet pressures, respectively and P_p is the permeate pressure. The transport of pure water through a membrane is by viscous flow. The membrane hydraulic resistance (R_m) can be described by Darcy's Law [17];

$$R_m = \frac{\text{TMP}}{\mu_w J_w} \quad (7)$$

where, J_w and μ_w are flux and viscosity of distilled water through the clean membrane, respectively.

At the end of each run, the distilled water flux of fouled membrane (J_{wf}) was measured for calculation of gel layer fouling resistance (R_g) using the following equation:

$$R_g = \frac{\text{TMP}}{\mu_{wf} J_{wf}} - R_m \quad (8)$$

where, μ_{wf} is the viscosity of distilled water through a fouled membrane. The concentration polarization resistance was then determined as:

$$R_{cp} = R_T - (R_g + R_m) \quad (9)$$

2.4. Statistical analysis

The analysis of variance (ANOVA) provides information about statistically significant factors. Analysis of variance of data was performed using statistical software called "MINITAB" release 13.20 (Minitab Inc., State College, USA), and determination of significant differences of means was carried out at 5% significant level.

2.5. ANN simulation

The most widely used ANN is the feed forward multilayer perceptron, where neurons are arranged into three layers: input layer, hidden layer and output layer. A schematic description of the 3-layers network structure used in this study is shown in Fig. 2. Each layer consists of several neurons. The number of input and output neurons corresponds to the number of input variables into the neural network and the number of desired output variables, respectively. There is at least one hidden layer between the input and the output layers that can have any number of neurons. The number of neurons in the hidden layer(s)

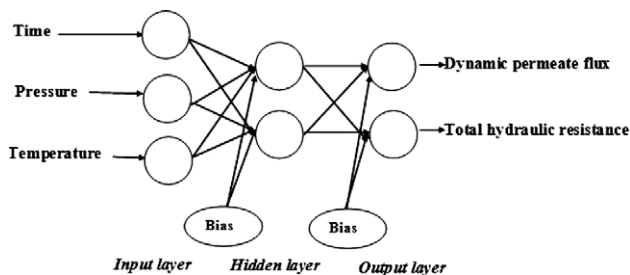


Fig. 2. Multilayer feed forward perceptron network architecture with one hidden layer for prediction of total hydraulic resistance and dynamic permeate flux of NF treatment of waste brine.

depends on the application of the network [18,19]. Each neuron is connected with all other neurons in the next layer by a weight connection. The inputs to the node are modified by interconnection weight and are determined as the weighted sum of its input [8,12].

Net input to the node in the hidden and output layer is obtained by adding a bias term with the weighted sum of the inputs. This process can be described by the following equation:

$$Y_j = \sum_{i=1}^n W_{ij} X_i + b_j \quad (10)$$

where x_i represents the input to a neuron, n is the number of input nodes, w_{ji} is the corresponding weight from i th to j th neurons and b_j is bias of the j th neuron. The expected output y_j is obtained via adjusting weights w_{ji} in the networks [20]. The reason for adding the bias term is that it allows a representation of phenomena having thresholds. Output from the node is determined by transforming this net input using a suitable transfer function. The transfer function can be linear or nonlinear (commonly sigmoidal and hyperbolic tangent) functions depending on the network topology [17,21]. In this work, the operational variables of NF treatment of waste brine (TMP, temperature and processing time) were used as inputs and dynamic flux and total hydraulic resistance as outputs. A sigmoid activation function (Eq. (11)) was chosen to be used as the transfer function in the hidden and output layers, due to lower calculated mean-squared error values comparing to the respective hyperbolic tangent function and linear function:

$$f(x) = \frac{1}{1 + e^{-x}} \quad (11)$$

The network architecture refers to the number of layers in the network and the number of neurons in each layer. The universal approximation theory suggests that a network with a single hidden layer with sufficient number of hidden neurons is able to map any input to any output to any degree of accuracy [14,22,23]. The ANN used in the present work featured with 1 hidden layer and bias nodes in the input and hidden layers. On the other hand, to find the best architecture, different networks were built with different hidden neurons.

In this study, 540 data were collected from experiments at different TMPs, temperatures and processing times. The data order was first randomized and then all data were divided into two sub-groups: first group including 360 data (2 TMP levels (1 & 2 MPa) \times 3

temperatures × 60 processing times) was used for developing ANNs model. For this purpose, 72 data were applied for training, and 288 data for cross validation. Another group including 180 data (1 TMP (1.5 MPa) × 3 temperatures × 60 processing times) was used as testing data to examine ANN predictability using data not used in the training and cross validation process (unseen data).

Training is the process by which the free parameters of the network (i.e. the weights) get optimal values. During training, the input and desired data will be repeatedly presented to the network. As the network learns, the error will drop toward zero. Cross validation is a highly recommended criterion for stopping the training of a network. The cross validating step was carried out with the best weights stored during the training. In this study, the fast Levenberg–Marquardt (LM) optimization technique was used to train the network [24]. Each predicted value was compared against the experimental value to test the network performance. For this purpose, three statistical parameters including mean square error (MSE), normalized mean square error (NMSE), and mean absolute error (MAE) were calculated to evaluate the prediction ability of network. On the lower values of MSE, NMSE and MAE, the network predicts more truly. In addition, the correlation coefficient (*r*), Eq. (12), gives information on the training of network, having a value between (−1, 1). If the correlation coefficient is close to (1), it shows how much the learning is successful.

$$r = \sqrt{1 - \frac{\sum_{i=1}^N [O_i - T_i]^2}{\sum_{i=1}^N [O_i - T_m]^2}} \quad (12)$$

where O_i is the *i*th actual value, T_i is the *i*th predicted value, N is the number of data, σ^2 is the variance and T_m is given by:

$$T_m = \frac{\sum_{i=1}^N O_i}{N} \quad (13)$$

In evaluating the network, various performance measures are computed. A sensitivity analysis was conducted to provide a measure of the relative importance among the inputs of the neural network model and to illustrate how the model output varied in response to variation of an input [25,26].

The Neurosolution software (Excel software release 6.0) was used for designing the neural networks and simulation of NF treatment of waste brine. This software incorporates various types of ANN presented by NeuroDimension, Inc., USA.

3. Results and discussion

3.1. NF performance

The experimental results obtained for NF treatment of waste brine are summarized in Table 2. It is found that the mean NaCl rejection, based on the conductivity, was ranged from 6.82 to 10.91% with the mean value as 9.19% and it decreased with increasing temperature. It means that about 81% of the salt was recovered and the feed was concentrated up to VCF9. A higher reduction on salt consumption was obtained in this work, 81% against 74% reported by Cartier et al. [2]. In addition, 90% reduction in water utilization was achieved. The colorant removal using NF process was in the range of 87.39–90.42% with the mean value as 89.31%, which is feasible completely for industrial purposes.

As it is shown in Table 2, the permeate flux was increased by increasing temperature and TMP and the maximum flux value (139.35 kg/m² h) was obtained at TMP 2 MPa and temperature 50°C. Furthermore, it can be found that the permeate flux increased almost 3.64 and 1.02% as the pressure and temperature

Table 2

Mean values of permeate flux and components rejection as a function of TMP and temperature (feed concentration 100 (g/l), pH 7.8 ± 0.1, $R_m = 4.46 \times 10^{13}$)

TMP (MPa)	Temperature (°C)	Flux (kg/m ² h)	NaCl rejection (%)	Colorant rejection (%)
1	30	82.14	10.91	88.90
1	40	96.63	9.09	87.39
1	50	114.69	6.82	89.27
1.5	30	103.57	9.55	89.76
1.5	40	109.37	9.55	90.42
1.5	50	123.18	8.64	90.40
2	30	127.39	10.00	90.35
2	40	133.73	10.00	87.86
2	50	139.35	8.18	89.66

increased by 0.1 MPa and 1°C, respectively. It seems that at such higher pressures, increasing the driving force led to increase in the flux, whereas, increasing the molecular diffusion and decreasing the viscosity led to flux improvement at such higher temperatures. In this study, the permeate flux was totally pressure-dependent in the pressure range studied.

The dynamic flux of waste brine NF process as a function of operating pressure and time is displayed in Figs. 3–5 at temperatures of 30, 40 and 50°C, respectively. These figures demonstrate that both initial flux and pseudo steady state flux (flux after about 10 min) vary significantly with TMP, temperature and time. It can be also observed that the flux decline was more pronounced at higher pressures; therefore the permeate flux was more stable at 1 MPa at all temperatures compared to other pressures studied. Abbas and Al-Bastaki [13] reported that the permeate rate increases with increasing pressure and temperature and decreases with increasing feed concentration. It is known that flux decline can be caused by several factors such as concentration polarization, gel layer formation and plugging of the pores. These entire factors cause additional resistances on the feed side to transport across the membrane [15]. The flux behavior during NF of resin wastewater was investigated by Cartier et al. [2]. In contrast, they observed a sharp flux decline from 701/h m² to 551/h m² during the first 170 min [2].

Flux decline due to fouling was evaluated by using the resistance-in-series model. Table 3 shows the values of fouling, total hydraulic resistance (R_T), concentration polarization resistance (R_{cp}) and gel layer resistance (R_g) as a function of TMP and temperature.

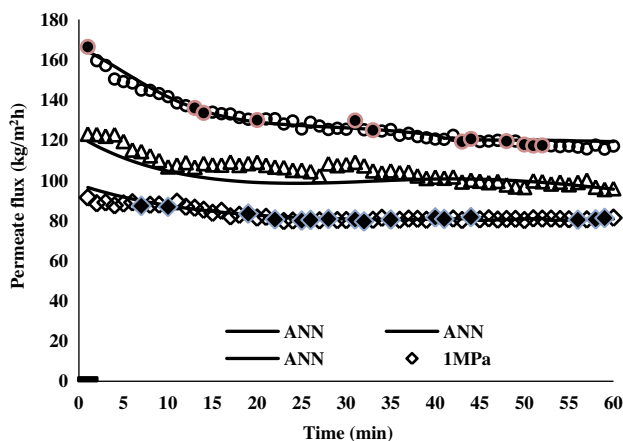


Fig. 3. The permeate flux vs. time, showing the experimental and the predicted values of NF treatment of waste brine by optimum ANN (3/9/2) configuration; Training points are shown by solid symbols (temperature 30°C).

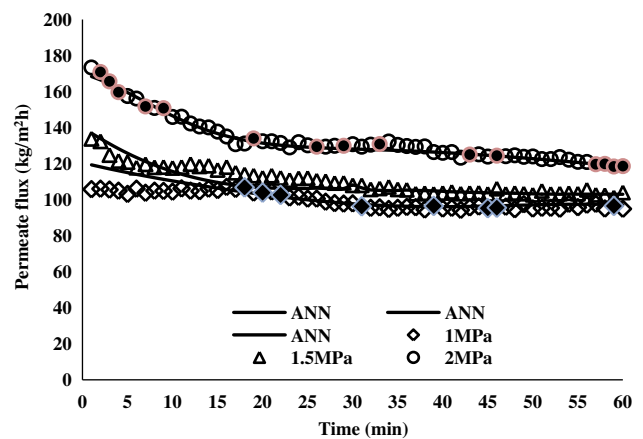


Fig. 4. The permeate flux vs. time, showing the experimental and the predicted values of NF treatment of waste brine by optimum ANN (3/9/2) configuration; Training points are shown by solid symbols (temperature 40°C).

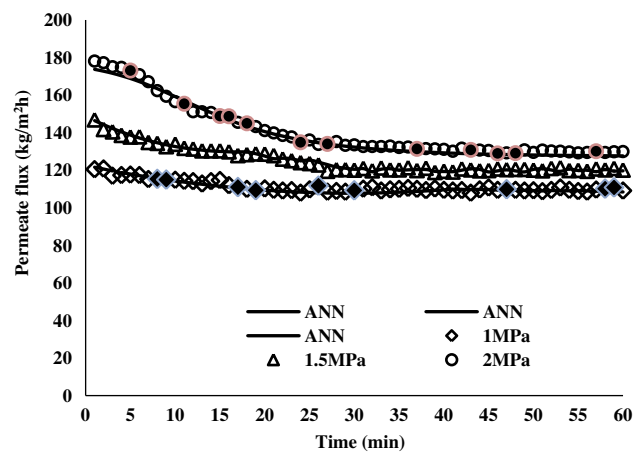


Fig. 5. The permeate flux vs. time, showing the experimental and the predicted values of NF treatment of waste brine by optimum ANN (3/9/2) configuration; training points are shown by solid symbols (temperature 50°C).

It can be seen that the average membrane fouling was ranged from 2.75 to 23.84% with the mean value as 12.97% and it increased greatly with increasing pressure. The results of fouling resistances (R_{cp} and R_g) also suggest the low membrane fouling propensity for this NF membrane surface because of a relatively stable flux behavior observed for most conditions. In this study, total hydraulic resistance, concentration polarization resistance and gel layer resistance were increased almost by 2.54, 8.21 and 7.49% with an increase of 0.1 MPa TMP; and 0.60, 1.84 and 2.23% with an increase of 1°C, respectively (Table 3).

Table 3

Mean values of fouling and hydraulic resistances (determined based on resistance-in-series model) as a function of TMP and temperature (feed concentration 100(g/l), pH 7.8 ± 0.1 , $R_m = 4.46 \times 10^{13}$)

TMP (MPa)	Temperature (°C)	Fouling (%)	R_T (m ⁻¹)	R_{CP} (m ⁻¹)	R_g (m ⁻¹)
1	30	3.75	4.94×10^{13}	2.02×10^{12}	2.80×10^{12}
1	40	2.75	4.97×10^{13}	1.01×10^{12}	4.08×10^{12}
1	50	3.96	5.00×10^{13}	1.95×10^{11}	5.20×10^{12}
1.5	30	10.15	5.53×10^{13}	3.66×10^{12}	7.05×10^{12}
1.5	40	21.27	6.04×10^{13}	9.91×10^{11}	1.48×10^{13}
1.5	50	13.65	6.30×10^{13}	7.05×10^{12}	1.13×10^{13}
2	30	14.28	5.99×10^{13}	5.32×10^{12}	1.00×10^{12}
2	40	23.08	6.59×10^{13}	2.57×10^{12}	1.87×10^{13}
2	50	23.84	7.42×10^{13}	1.02×10^{13}	1.94×10^{13}

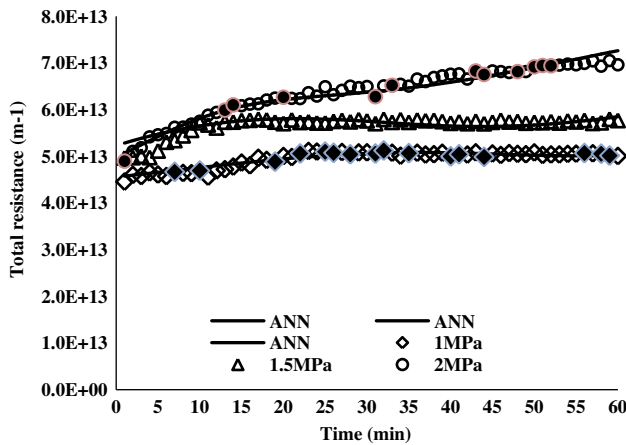


Fig. 6. The total hydraulic resistance vs. time, showing the experimental and the predicted values of NF of waste brine by optimum ANN (3/9/2) configuration; training points are shown by solid symbols (temperature 30°C).

The effects of the applied TMP, temperature and time on total hydraulic resistance of waste brine NF process are presented in Figs. 6–8. The results with the polyamide membrane under various temperatures showed that R_T increased with time at all TMPs. It can be seen that fouling was more pronounced at higher pressures, same as the results observed for permeate flux (Figs. 3–5). Based on experimental works of this study, the gel layer formed on the membrane surface was in principle reversible by rinsing with pure water.

The results of analysis variance obtained for permeate flux, fouling, colorant rejection and NaCl rejection are given in Table 4. The ANOVA approach was applied to investigate which factors significantly affect the response parameters. Statistical analysis displayed that the permeate flux was significantly affected by pressure, temperature and interaction between pressure and temperature ($p < 0.01$), whereas the fouling

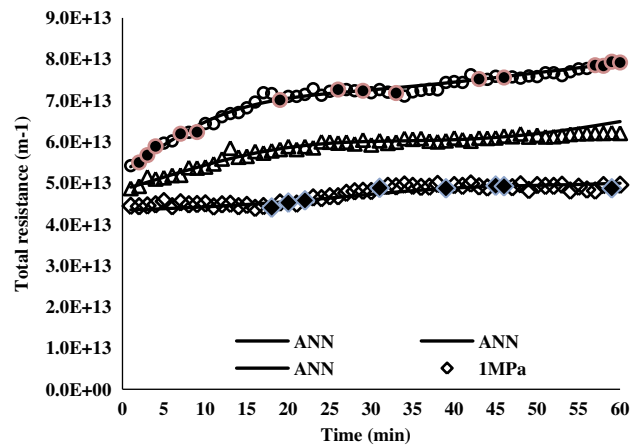


Fig. 7. The total hydraulic resistance vs. time, showing the experimental and the predicted values of NF of waste brine by optimum ANN (3/9/2) configuration; training points are shown by solid symbols (temperature 40°C).

and NaCl rejection was significantly influenced by pressure and temperature, respectively ($p < 0.01$). Furthermore, the studied variables had no significant effect on colorant rejection of waste brine NF process.

3.2. Simulation results

In this work, the applications of neural network approach for dynamic prediction of permeate flux and total hydraulic resistance were tested for NF treatment of waste brine at different TMPs and temperatures.

The training process was carried out for 1,000 iterations or until the cross-validation data's mean-squared error (MSE) did not improve for 100 iterations to avoid over-fitting of the network. Errors values obtained for estimation dynamic flux and total hydraulic resistance during the testing step are shown in Table 5. It was found that the ANN with nine

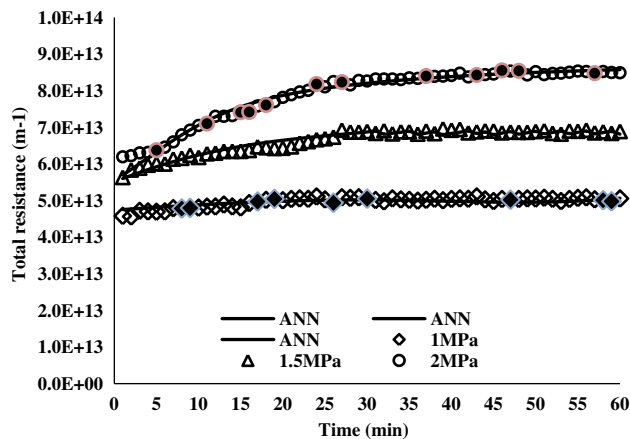


Fig. 8. The total hydraulic resistance vs. time, showing the experimental and the predicted values of NF of waste brine by optimum ANN (3/9/2) configuration; training points are shown by solid symbols (temperature 50°C).

hidden neurons had the minimum NMAE values (0.06 and 0.05) for dynamic flux and total hydraulic resistance prediction, respectively. Therefore, this architecture can be selected as the best ANN.

Table 6 illustrates the weight and bias values of the selected ANN, which could be used to predict dynamic flux and total hydraulic resistance of NF treatment of waste brine. The efficiency of the selected ANN model for prediction of unseen dynamic flux data (TMP = 1.5 MPa at three levels of temperature) is presented in Figs. 3–5. It can be seen that the dynamic flux, J_P , was well predicted by the best ANN configuration (3/9/2).

The total hydraulic resistance, R_T , was estimated from Eq. (5). The experiments with varying TMP and temperature were carried out to investigate membrane fouling. The experimental data and the results of modeling using ANNs for the total hydraulic resistance (R_T) at all TMPs and temperature are shown in

Figs. 6–8. Figs. 3–8 show that the complex behavior (non-linearity) of J_P -time or R_T -time profile is well reproduced by the ANNs. As shown in Figs. 3–8, there is excellent agreement between the predictions and the experimental data of full time-dependent J_P/R_T profiles at TMP 1 and 2 MPa and also for unseen data (TMP = 1.5 MPa) at all temperatures.

The calculated correlation coefficient values for estimation of dynamic flux and total hydraulic resistance were 0.96 and 0.98, respectively, which show high correlation between predicted and experimental values (Table 5). The ability to predict J_P and R_T at intermediate TMP (1.5 MPa) could reduce the computation time and the amount of practical work required before designing a new membrane process. Thus, these results suggest that in actual practice, the maximum information and great saving in time and cost can be obtained with a minimum number of experiments.

Sensitivity analysis was tested in order to study the sensitiveness of neural network models toward different inputs (Figs. 9 and 10). It can be found that among the input variables, pressure was the most sensitive factor for prediction of both flux and total hydraulic resistance by the selected ANN.

4. Conclusions

1. The results display satisfactory qualitative performance of NF membranes treatment for the removal of colorant components (89%) and high recovery of salts (81%) and water (90%) for reuse from the resin regeneration waste. The mean rejection of sodium chloride was found to be 9%. Permeate flux, membrane fouling and NaCl rejection increased significantly when pressure and temperature increased, respectively. The average membrane fouling was found to be 13%. The results showed that the total hydraulic resistance, concentration polarization

Table 4

Successive mean squares from the analysis of variance of the flux, NaCl rejection, colorant rejection and fouling of two operation parameters

Source	Degree of freedom	Mean square			
		Flux (kg/m ² h)	Fouling (%)	Colorant rejection (%)	NaCl rejection (%)
TMP	2	1934.68*	448.06*	4.227 ^{NS}	0.322 ^{NS}
Temperature	2	691.88*	62.82 ^{NS}	2.754 ^{NS}	8.327*
TMP × temperature	4	57.37*	29.57 ^{NS}	1.418 ^{NS}	1.426 ^{NS}
Error	9	5.84	21.07	4.519	1.472
Total	17				

Note: * $p=0.01$; NS, not significant.

Table 5

Errors values in prediction of dynamic flux and total hydraulic resistance of NF treatment of waste brine using ANN (3/9/2)

Performance	Dynamic flux	Total hydraulic resistance
MSE (mean squared error)	24.57	6.82×10^{24}
NMSE (normalized mean squared error (MSE/variance of desired output))	0.06	0.05
MAE (mean absolute error)	3.27	1.64×10^{12}
Minimum absolute error	0.03	1.53×10^{10}
Maximum absolute error	16.53	9.47×10^{12}
Correlation coefficient	0.958	0.980

Table 6

Corresponding weight and bias values of each neuron for optimum ANN configuration selected to predict dynamic permeate flux and total hydraulic resistance of regeneration waste brine

Hidden neurons	Bias	Input neurons			Output neurons	
		Time	TMP	Temperature	Dynamic flux	Total resistance
1	-0.0206	1.6074	0.7886	0.0634	0.5585	0.5172
2	-0.8872	-0.3628	-0.3704	-0.5922	-0.4536	0.3706
3	0.7103	-0.811	1.1384	-1.2030	0.5655	0.9745
4	-1.0287	-1.3034	-1.1099	1.6665	0.7013	0.8232
5	0.7036	-0.1789	0.6468	-0.0178	1.756	-0.4175
6	1.0926	-0.3025	0.1182	0.8615	-0.2434	-0.245
7	0.4511	-0.1978	-0.3665	-0.5119	-0.4425	0.5953
8	0.4655	-0.3127	0.7738	-0.2423	-0.9946	-2.025
9	-2.7587	-1.8942	0.9734	0.1649	0.2543	-1.091
Bias					0.5363	-0.4841

resistance and gel layer resistance increased with increasing TMP and temperature.

2. The application of ANNs to the simulation of crossflow NF was investigated to predict the dynamic

behavior of permeate flux and total hydraulic resistance (as outputs) vs. pressure, temperature and time (as inputs). A sigmoid transfer function was used for the hidden and output layers. The results suggest that

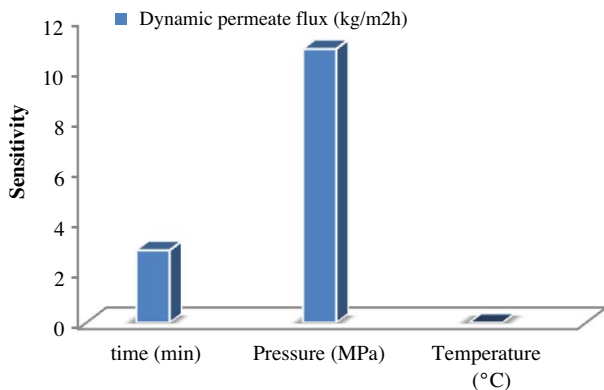


Fig. 9. Sensitivity of the best selected ANN (3/9/2) toward the inputs for prediction of dynamic permeate flux.

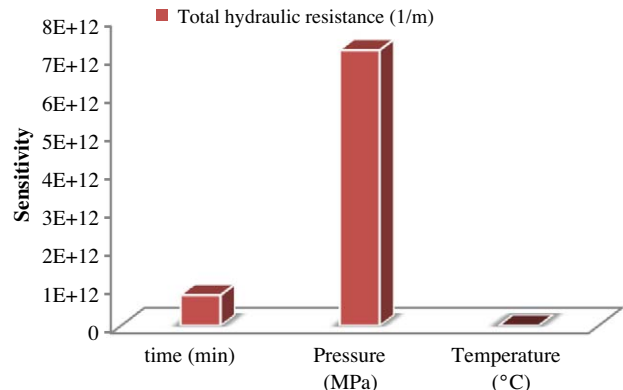


Fig. 10. Sensitivity of the best selected ANN (3/9/2) toward the inputs for prediction of total hydraulic resistance.

an optimum ANN model with 3/9/2 configuration could potentially be used to accurately simulate the dynamic behavior of permeate flux and total hydraulic resistance of NF treatment of waste brine ($r=0.96$ and $r=0.98$, respectively).

Symbols

b_j	—	bias
C_f	—	feed concentration, g/L
C_p	—	permeate concentration, g/L
J_p	—	permeate flux, $\text{kg/m}^2 \text{h}^{-1}$
J_w	—	distilled water flux before run, $\text{kg/m}^2 \text{h}^{-1}$
J_{wf}	—	distilled water flux after run, $\text{kg/m}^2 \text{h}^{-1}$
P_i	—	inlet pressures, MPa
P_o	—	outlet pressures, MPa
P_p	—	permeate pressure, MPa
R_{cp}	—	concentration polarization resistance, m^{-1}
R_g	—	gel layer resistance, m^{-1}
R_m	—	membrane resistance, m^{-1}
R_T	—	total hydraulic resistance, m^{-1}
TMP	—	transmembrane pressure, MPa
VRF	—	volume reduction factor
V_f	—	initial volume of feed, L
V_c	—	final volume of the concentrate, L
w	—	weight
x_i	—	input to a neuron
y_j	—	output
$\Delta\pi$	—	osmotic pressure differences, MPa
μ_p	—	permeate viscosity, Pa s
μ_w	—	distilled water viscosity, Pa s
μ_{wf}	—	distilled water viscosity through a fouled membrane, Pa s

References

- [1] A. Hinkova, Z. Bubník, P. Kadlec, J. Pridal, Potentials of separation membranes in the sugar industry, *Sep. Purif. Technol.* 26 (2002) 101–110.
- [2] S. Cartier, M.A. Theoleyre, M. Decloux, Treatment of sugar decolorizing regeneration waste using nanofiltration, *Desalination* 113 (1997) 7–17.
- [3] S. Wadley, C.J. Brouckaert, L.A.D. Baddock, C.A. Buckley, Modelling of nanofiltration applied to the recovery of salt from waste brine at a sugar decolorisation plant, *J. Membr. Sci.* 102 (1995) 163–175.
- [4] R.J. Petersen, Composite reverse osmosis and nanofiltration membranes, *J. Membr. Sci.* 83 (1993) 81–150.
- [5] N.A. Darwish, N. Hilal, H. Al-Zoubi, A.W. Mohammad, Neural networks simulation of the filtration of sodium chloride and magnesium chloride solutions using nanofiltration membranes, *I. Chem. E* 85 (2007) 417–430.
- [6] S.J. Duranceau, Modeling the permeate transient response to perturbations from steady-state in a nanofiltration process, *Desalin. Water Treat.* 1 (2009) 7–16.
- [7] I.S. Chang, R. Field, Z. Cui, Limitations of resistance-in-series model for fouling analysis in membrane bioreactors: A cautionary note, *Desalin. Water Treat.* 8 (2009) 31–36.
- [8] B. Sarkar, A. Sengupta, S. De, S. DasGupta, Prediction of permeate flux during electric field enhanced cross-flow ultrafiltration—a neural network approach, *Sep. Purif. Technol.* 65 (2009) 260–268.
- [9] M. Dornier, M. Decloux, G. Trystram, A. Lebert, Dynamic modeling of crossflow microfiltration using neural networks, *J. Membr. Sci.* 98 (1995) 263–273.
- [10] C. Teodosiu, D. Pastravanu, M. Macoveanu, Neural network model for ultrafiltration and backwashing, *Water Res.* 34 (2000) 4371–4380.
- [11] T.M. Hwang, Y. Choi, S.H. Nam, S. Lee, H. Oh, K. Hyun, Y. K. Choung, Prediction of membrane fouling rate by neural network modeling, *Water Treat.* 15 (2010) 134–140.
- [12] S.M.A. Razavi, S.A. Mortazavi, S.M. Mousavi, Dynamic modelling of milk ultrafiltration by artificial neural network, *J. Membr. Sci.* 220 (2003) 47–58.
- [13] A. Abbas, N. Al-Bastaki, Modeling of an RO water desalination unit using neural networks, *Chem. Eng. J.* 114 (2005) 139–143.
- [14] W.R. Bowen, M.G. Jones, J.S.T. Welfoo, H.N. Yousef, Predicting salt rejections at nanofiltration membranes using artificial neural networks, *Desalination* 129 (2000) 147–162.
- [15] S.C. Tu, V. Ravindran, M. Pirbazari, A pore diffusion transport model for forecasting the performance of membrane processes, *J. Membr. Sci.* 265 (2005) 9–50.
- [16] Y. Kaya, H. Barlasa, S. Arayici, Evaluation of fouling mechanisms in the nanofiltration of solutions with high anionic and nonionic surfactant contents using a resistance-in-series model, *J. Membr. Sci.* 367(1–2) (2011) 45–54.
- [17] A.K. Pabby, S.S.H. Rizvi and A.M. Sastre, *Handbook of Membrane; Separations Chemical, Pharmaceutical, Food, and Biotechnological Applications*, Taylor & Francis Group, New York, NY, 2009.
- [18] S.M.A. Razavi, S.A. Mortazavi, S.M. Mousavi, Application of neural networks for crossflow milk ultrafiltration simulation, *Int. Dairy J.* 14 (2004) 69–80.
- [19] N. Hilal, O.O. Ogunbiyi, M. Al-Abri, Neural network modeling for separation of bentonite in tubular ceramic membranes, *Desalination* 228 (2008) 175–182.
- [20] Q. Liu, S. Kim, S. Lee, Prediction of microfiltration membrane fouling using artificial neural network models, *Sep. Purif. Technol.* 70 (2009) 96–102.
- [21] M. Fathi, M. Mohebbi, S.M.A. Razavi, Application of image analysis and artificial neural network to predict mass transfer kinetics and color changes of osmotically dehydrated kiwifruit, *Food Bioprocess Technol.* (2009), doi: 10.1007/s11947-009-0222-y.
- [22] S.S. Tambe, B.D. Kulkarni and P.B. Deshpande, *Elements of artificial neural networks with selected applications in chemical engineering, and chemical and biological sciences, Simulation and Advanced Controls*, Louisville, KY, 1996.
- [23] S. Chellam, Artificial neural network model for transient crossflow microfiltration of polydispersed suspensions, *J. Membr. Sci.* 258 (2005) 35–42.
- [24] M.T. Hagan, M. Menhaj, Training feed forward networks with the Marquardt algorithm, *IEEE. Trans. Neural Network* 5 (1994) 989–993.
- [25] M.P. Rapetto, A. Almqvist, R. Larsson, P.M. Lugt, On the influence of surface roughness on real area of contact in normal, dry, friction free, rough contact by using a neural network, *Wear* 266(5–6) (2009) 592–595.
- [26] A. Mohebbi, M. Taheria, A. Soltania, A neural network for predicting saturated liquid density using genetic algorithm for pure and mixed refrigerants, *Int. J. Refrig.* 31(8) (2008) 1317–1327.